

# Capillary Force-Induced Glue-Free Printing of Ag Nanoparticle Arrays for Highly Sensitive SERS Substrates

Jaehong Lee,<sup>†</sup> Jungmok Seo,<sup>†</sup> Dayeong Kim,<sup>†</sup> Sera Shin,<sup>†</sup> Sanggeun Lee,<sup>†</sup> Chandreswar Mahata,<sup>†</sup> Hyo-Sung Lee,<sup>‡</sup> Byung-Wook Min,<sup>‡</sup> and Taeyoon Lee<sup>\*,†</sup>

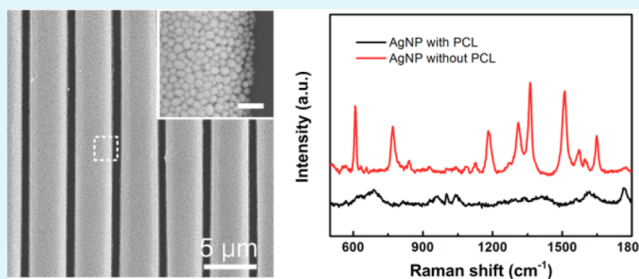
<sup>†</sup>Nanobio Device Laboratory, School of Electrical and Electronic Engineering, Yonsei University, 50 Yonsei-ro, Seodaemun-Gu, Seoul 120-749, Republic of Korea

<sup>‡</sup>Microwave Integrated Circuits and Systems Laboratory, School of Electrical and Electronic Engineering, Yonsei University, 50 Yonsei-ro, Seodaemun-Gu, Seoul 120-749, Republic of Korea

## S Supporting Information

**ABSTRACT:** The fabrication of well-ordered metal nanoparticle structures onto a desired substrate can be effectively applied to several applications. In this work, well-ordered Ag nanoparticle line arrays were printed on the desired substrate without the use of glue materials. The success of the method relies on the assembly of Ag nanoparticles on the anisotropic buckling templates and a special transfer process where a small amount of water rather than glue materials is employed. The anisotropic buckling templates can be made to have various wavelengths by changing the degree of prestrain in the fabrication step. Ag nanoparticles assembled in the trough of the templates via dip coating were successfully transferred to a flat substrate which has hydrophilic surface due to capillary forces of water. The widths of the fabricated Ag nanoparticle line arrays were modulated according to the wavelengths of the templates. As a potential application, the Ag nanoparticle line arrays were used as SERS substrates for various probing molecules, and an excellent surface-enhanced Raman spectroscopy (SERS) performance was achieved with a detection limit of  $10^{-12}$  M for Rhodamine 6G.

**KEYWORDS:** nanoparticle assembly, Ag nanoparticles, buckling structure, SERS, dip coating, nanoparticle transfer using wettability, glue-free transfer



## INTRODUCTION

Over the past decade, 1-dimensional (1-D), 2-dimensional (2-D), and 3-dimensional (3-D) ordered structures of nanoparticles have attracted a massive amount of interest due to their potential applications as photonic band gap materials,<sup>1</sup> high-efficient sensors,<sup>2,3</sup> low-cost solar cells<sup>4</sup> and sacrificial templates for lithography.<sup>5–7</sup> To realize such applications, the successful assembly of nanoparticles into a well-ordered structure on desired surfaces is very crucial since randomly aggregated nanoparticles could hinder specific properties of the assembled nanoparticles, including plasmonic coupling effects,<sup>8</sup> optical bandgaps,<sup>9</sup> and metamaterial effects.<sup>10</sup>

To ensure the self-assembly of colloidal metal nanoparticles into well-ordered 1-D, 2-D, and 3-D structures, various methods such as sedimentation,<sup>11</sup> evaporation,<sup>12</sup> use of external electric fields<sup>13</sup> and electrostatic potential,<sup>14</sup> electrochemical deposition,<sup>15</sup> block copolymer micelle nanolithography,<sup>16</sup> and template-assisted approaches<sup>17–20</sup> have been extensively investigated and some progress has been reported. Among the techniques, template-assisted approaches have been widely employed to obtain closed-packed nanoparticle arrays. Although the template-assisted technique may require an additional transfer process, it has important advantages in

terms of cost-effectiveness, controllability and assembly precision in macroscopic dimensions compared to other approaches.<sup>21–23</sup> In contrast to our technique, assembling of nanoparticles using electron beam lithography not only requires expensive equipment with complicated procedures but also is not suitable to achieve an assembled structure over a large area.<sup>24</sup> On the other hand, self-assembly methods have limited structural controllability compared to the template-assisted technique.<sup>21</sup> In the template-assisted approaches, nanoparticles dispersed in suspension can be well-aligned into predefined, topographically structured surfaces such as grooves, micro-molds and trenches by the hydrodynamic flow of the solvent. However, in order to utilize such methods in practical aspects, nanoparticle arrays assembled on the predefined templates should be transferred to the desired flat substrate. Ling et al. investigated an assembly process for a 3-D structure of polystyrene (PS) particles using a poly(dimethylsiloxane) (PDMS) mold and a transfer process to a flat surface with the help of a surface chemical treatment.<sup>25</sup> Jeong and co-

Received: January 3, 2014

Accepted: May 13, 2014

Published: May 13, 2014

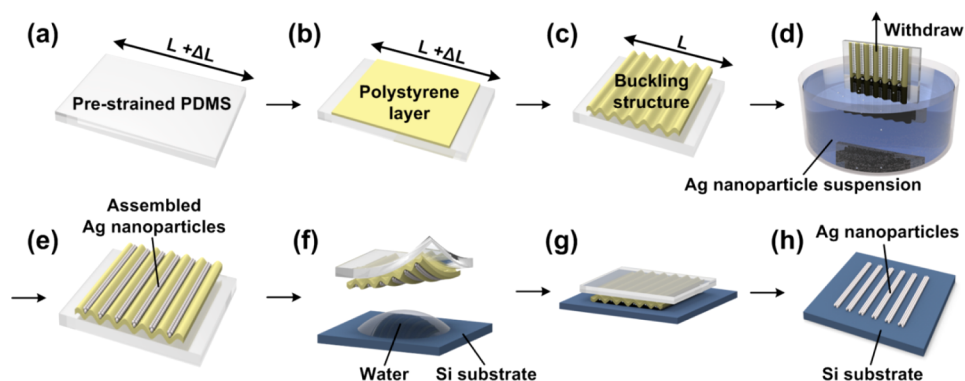


**Figure 1.** Fabrication process used to assemble glue-free Ag nanoparticle line arrays on a flat substrate: (a–c) procedure to obtain anisotropic buckling templates, (d and e) assembly of Ag nanoparticles onto a template, and (f–h) transfer of Ag nanoparticle line arrays onto the desired substrate.

workers demonstrated a reversible assembly process where patterned colloidal arrays could be fabricated on a flat surface through the use of a PS buckling structure.<sup>26</sup> Although a colloidal assembly and printing with good controllability were achieved, the inevitable need for a surface treatment and the use of glue materials in the process may have a detrimental influence on synthesized structures for several bioanalysis and biosensor applications.<sup>27</sup> As an application of assembled nanoparticles, a lot of research effort has been made to develop functional metallic and plasmonic arrays for SERS applications. Since the performance of SERS substrates such as accuracy of quantitative analysis and reproducibility are generally inferior because of random distributions of metal nanoparticles,<sup>28</sup> periodicity of metallic nanoparticle arrays is an elegant way to obtain high reproducibility and quantitative analysis.<sup>29</sup>

In this Research Article, we demonstrate a facile approach to assemble Ag nanoparticles onto a predefined buckling structure and transfer the assembled Ag nanoparticle arrays without any glue material. Anisotropic buckling structures were used to prepare topologically patterned templates by releasing the strain of mechanically prestretched PDMS substrates with a transferred PS layer. Ag nanoparticle suspension were synthesized via the polyol process and assembled on a topographically patterned template in microscopic line arrays by dip-coating. The wavelengths of the anisotropic buckling structure could be adjusted by changing the degree of prestrain in the prestretched PDMS substrate, and the corresponding widths of the assembled nanoparticle line arrays also could be manipulated. Patterned line arrays of Ag nanoparticles were successfully printed onto a desired flat substrate without glue materials using the capillary forces of water. Because the capillary forces were mainly related to the difference between the surface tension of the solution and the substrate, it was confirmed that the aspects of the Ag nanoparticle line arrays transferred onto the desired substrates were changed according to the surface wettability of the substrate. As a proof-of-concept, we demonstrated the performance of the glue-free line arrays of Ag nanoparticles as a SERS substrate.

## EXPERIMENTAL SECTION

**Synthesis of Ag Nanoparticles.** Five milliliters of ethylene glycol was first heated for 1 h at 152 °C. Then, 1.5 mL of a 94 mM Ag nitrate ( $\text{AgNO}_3$ ) solution mixed with 1.5 mL of a 147 mM polyvinylpyrrolidone (PVP) solution was added into the preheated ethylene glycol, and stirred for 30 min. This sample

was cooled to room temperature and, diluted with acetone, and the synthesized Ag nanoparticles were centrifuged at 3500 rpm for 20 min to remove the ethylene glycol. Then the Ag nanoparticles diluted with methanol were centrifuged at the same conditions several times to remove unreacted PVP residues. The elimination of PVP residues was demonstrated by measuring Fourier transform infrared (FTIR) spectroscopy of Ag nanoparticles after multiple centrifugation steps as shown Figure S1 in Supporting Information. Finally, the synthesized Ag nanoparticles were dispersed in 5 mL of deionized water (DI water).

**Preparation of an Anisotropic Buckling Template.** Flat PDMS substrates were prepared by mixing a Sylgard 184 base and its curing agent in a 20:1 (base:curing agent) volume composition. After it was mixed, the solution was kept at room temperature overnight and then heated at 80 °C for 12 h. PS thin films were prepared by spin-coating a 1% PS solution dissolved in toluene onto an oxygen plasma-treated Si wafer. After the PDMS substrate was mechanically stretched in one direction, the PS thin films on Si were placed in contact with the prestretched PDMS substrate and then immersed in DI water to separate the Si wafer from the PS layer. After 5 min, the Si wafer was removed and release of strain in the PDMS substrate created anisotropic buckling of the PS thin film.

**Assembly and Transfer of Ag Nanoparticles.** A dip-coating process was used to assemble Ag nanoparticles onto the anisotropic buckling template. Prior to dip-coating, the buckling template was exposed to oxygen plasma (40 W, 2 sccm, 50 s). The template was immersed in the Ag nanoparticles solution such that the line patterns of the template were perpendicular to the surface of the solution. The template was then withdrawn vertically at the speed of 0.012 mm/min. For the transfer of Ag nanoparticles, a cleaned Si wafer was treated with oxygen plasma (70 W, 2 sccm, 180 s) to produce a hydrophilic surface. Ten microliters of water was then dropped onto the cleaned wafer and the template filled with Ag nanoparticles was placed onto the droplet. After it was dried overnight to eliminate water, the template was removed from the substrate. To confirm the effect of the surface wettability of the Si wafer in the transfer process, the surface of the Si was modified by immersing it in a 3 mM solution of dodecyltrichlorosilane (DTS) dissolved in toluene for 20 min at room temperature; the details of this process are described elsewhere.<sup>30,31</sup> The samples were then annealed at 120 °C for 15 min. For the preparation of Ag nanoparticle line arrays with glue materials, poly( $\epsilon$ -caprolactone) (PCL) films were produced by spin-

coating a PCL solution in toluene (3 wt %) at 1500 rpm for 60 s on Si wafers. The stretched buckling templates containing Ag nanoparticle arrays were placed on top of the PCL layer, which was preheated to 65 °C in a conformal manner.

**SERS Measurements.** Rhodamine 6G (R6G), Nile blue A (NBA), and 1,2-bis(4-pyridyl)ethylene (BPE) were used as probing molecules for SERS measurements. For the preparation of SERS-active substrates, fabricated samples of Ag nanoparticle line arrays were immersed in R6G, NBA, and BPE solutions of  $10^{-3}$ ,  $10^{-6}$ ,  $10^{-9}$ , and  $10^{-12}$  M for 24 h and then dried under nitrogen flow. Since the excess solutions on the substrates can be completely removed through nitrogen flow after the dipping process, the probing molecules-coated SERS substrates without excess molecules can be obtained using the dipping step. Also, during the dipping step of substrates in these solutions, diffusion of Ag nanoparticles in the line arrays does not occur due to enhanced adhesion force between each nanoparticle. (Figure S2 in Supporting Information) He–Ne laser (633 nm) was used as a light source and a laser power of 20  $\mu$ W was employed for 1 s. SERS spectra were obtained using a HORIBA Lab Ram ARAMIS Raman spectrometer. Excitation light was focused on the samples using a 100 $\times$  microscope objective (Olympus microscope) and a diffraction grating of 600 gr/mm.

**Characterization.** Surface morphologies were examined using a JEOL JSM-7001F field emission scanning electron microscope (FE-SEM) and a Park System XE-100 atomic force microscope (AFM). FTIR spectrum was measured with Bruker Vertex 70 FT-IR Spectrometer.

## RESULTS AND DISCUSSION

Figure 1 illustrates the procedure for printing Ag nanoparticles arrays on a flat substrate. This procedure involves three main steps: fabrication of anisotropic buckling template, assembly of Ag nanoparticles onto the template and transfer of the Ag nanoparticle line arrays onto a flat substrate. Figure 1a–c schematically illustrates the process for fabricating an anisotropic buckling template. A 70 nm-thick PS layer was transferred from a hydrophilic Si wafer to a 2 mm-thick prestrained PDMS substrate in one direction. To transfer the PS layer, the hydrophilic Si wafer coated with the PS layer was placed onto the prestrained PDMS substrate, and the structure was immersed in DI water for 5 min. During this step, the PS layer was successfully separated from the wafer since water can infiltrate into the interface between the hydrophilic wafer and the hydrophobic PS layer. After 5 min, the strain in the prestrained PDMS substrate with the transferred PS layer was released, thereby generating uniform anisotropic buckling patterns on the PS layer. To assemble the Ag nanoparticles in solution onto the troughs of the anisotropic buckling template, the dip-coating process was employed as shown in Figure 1d and e. Prior to dip-coating, the anisotropic buckling template was slightly treated with oxygen plasma treatment to induce a hydrophilic surface. The template was then immersed in the Ag nanoparticle solution with the direction that its line patterns were parallel to the vertically withdrawing direction. By withdrawing at a uniform rate, Ag nanoparticles could be selectively deposited into the troughs of the template. Figure 1f–h illustrates the transfer process for assembled Ag nanoparticles from the buckling template to a flat substrate. In this transfer process, a small amount of water was used to achieve successful transfer of the Ag nanoparticles without any glue materials that are generally employed to provide adhesion

between the substrate and the particles in typical transfer processes. Ten microliters of water was dropped onto the hydrophilic flat substrate and then the buckling template containing the assembled Ag nanoparticles was placed on the small amount of water until the water was evaporated completely as shown in Figure 1f and g. Through this transfer process, Ag nanoparticle line arrays were successfully transferred onto the desired substrate without any glue materials, which mostly have detrimental effects in a wide range of applications, including chemical or biological sensors, optical and electrical unit.

The Ag nanoparticles employed in this work were synthesized by the polyol process,<sup>32</sup> where ethylene glycol acted as both a reductant and a solvent for Ag ions. Through heating process, most of the Ag ions in the ethylene glycol were reduced to twinned or multiply twinned particles (MTPs) that have surfaces bounded by lowest-energy {111} facets. On the nanometer scale, reduced metal ions mainly prefer to nucleate and grow into MTPs, which generally have a trigonal and lamella shape.<sup>33</sup> Therefore, chemical capping reagents have to be added in the synthesis process to obtain other morphologies, including spheres with less stable facets.<sup>34</sup> When the capping agent, PVP, was introduced, the selective interaction between PVP and the planes of the silver MTPs adjusted the growth rate of the silver MTPs according to the directions of planes. Through the use of PVP, Ag nanoparticles with a spherical shape were successfully synthesized. Figure 2a shows an SEM

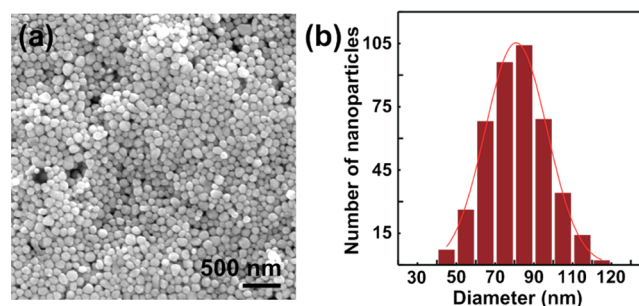


**Figure 2.** (a) Typical SEM image showing the Ag nanoparticles synthesized via the polyol process. (b) Histogram of the diameter distribution of the Ag nanoparticles.

image of the synthesized Ag nanoparticles, which have an average diameter of 82 nm, with a standard deviation of 16 nm. The diameter distribution of the Ag nanoparticles is displayed in Figure 2b.

Figure 3a and b provide AFM and optical microscopy images showing the anisotropic buckling structures obtained by applying a 35% uniaxial mechanical strain on the PDMS substrate. By releasing the mechanical prestrain, uniaxial compressive stress created periodic buckling patterns based on the difference between the Young's modulus of the PDMS substrate and the PS layer. Figure 3c shows a cross-sectional graph of the obtained buckling structures, taken along the line A–A' shown in Figure 3b. It is evident that the obtained buckling structures have uniform wavelengths and heights. The uniform buckling structure was well formed over the entire area of the PS layer, as shown in Figure 3d. Although a few  $\gamma$ -shape defects were generated in the PS buckling structure, the negative effects of these  $\gamma$ -shape defects on the whole sample were negligible since the defects were intrinsic to the fabrication process<sup>35</sup> and the area covered by the defects was much smaller

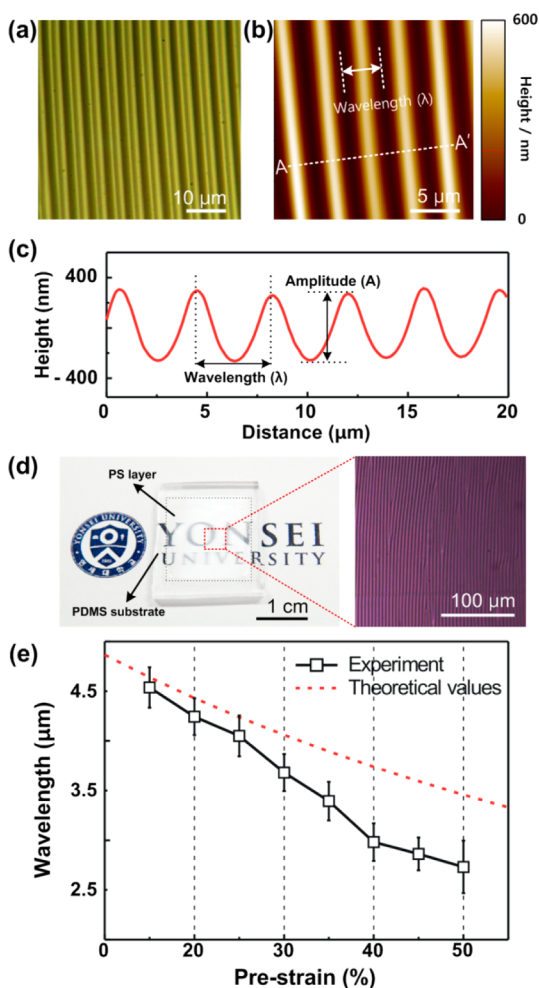


**Figure 3.** Anisotropic buckling structure of the PS layer on the PDMS substrate: (a) optical image, (b) its corresponding AFM image, and (c) topography of the cross section at a prestrain degree of 35%. (d) Photograph image (left) and the corresponding optical image (right) of PS buckling structures on PDMS substrates. The Yonsei University logo is reprinted with permission from Yonsei University. (e) The measured and theoretical values of the wavelengths of the buckling structure as the prestrain degree is varied.

than the buckling structured regions. The patterns were perpendicular to the stretching direction of the PDMS substrate, and the mean wavelength of the buckling structure was  $3.39 \mu\text{m}$ . This value is comparable to the theoretically estimated one,  $3.89 \mu\text{m}$ , obtained from an equation based on finite deformation buckling theory.<sup>35</sup> According to the finite deformation buckling theory, the wavelength of a buckling structure is

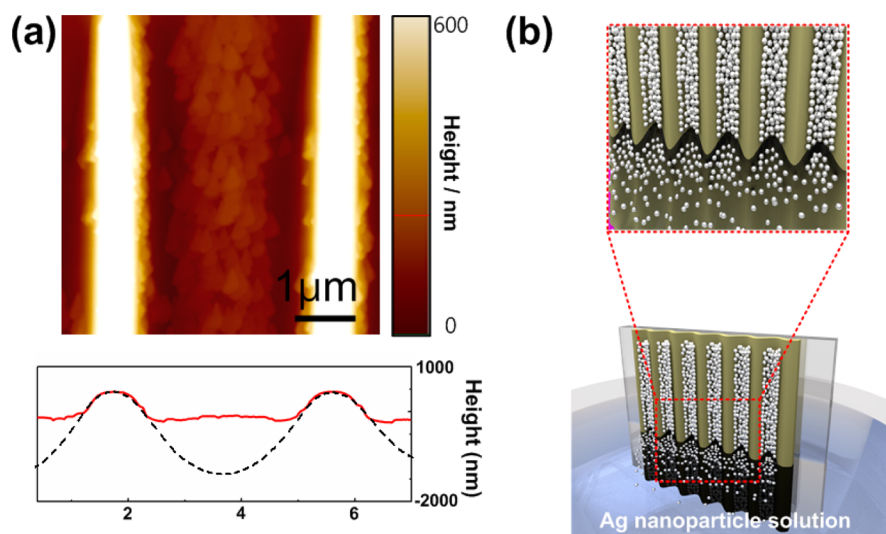
$$\lambda = \frac{\lambda_0}{(1 + \varepsilon_{\text{pre}})(1 + 5\varepsilon_{\text{pre}}(1 + \varepsilon_{\text{pre}}/32))^{1/3}} \left( \lambda_0 \right) = 2\pi h \left( \frac{E_f(1 - \nu_s^2)}{3E_s(1 - \nu_f^2)} \right) \quad (1)$$

where  $h$  is the thickness of the PS layer with an elastic modulus  $E_f$  of 3.5 GPa, Poisson's ratio  $\nu_f$  of 0.35, while  $\varepsilon_{\text{pre}}$  is the degree of prestrain in the stretched PDMS substrate with a Young's modulus  $E_s$  of 0.51 MPa and Poisson's ratio  $\nu_s$  of 0.48. The wavelengths of the buckling structures depend on the prestrain

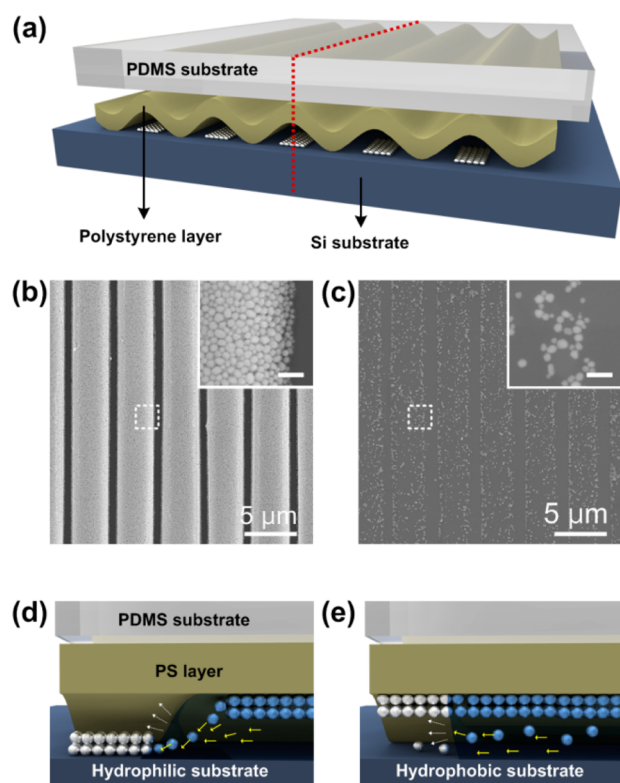
degree imposed on the elastomeric substrate in agreement with eq 1. Figure 3e shows the wavelengths of the buckling structure for various prestrain degrees. As the degree of prestrain in the PDMS substrate increases, the wavelength of the buckling structure tends to be reduced; this relation corresponds well to the finite deformation buckling theory. By modulating the wavelengths of the anisotropic buckling templates, the width of the Ag nanoparticle line arrays transferred onto the flat substrates can be readily controlled. Supporting Information Figure S3 shows typical SEM images of Ag nanoparticle line arrays on flat substrates obtained when various templates with buckling structures of different wavelengths are used. The buckling templates employed to fabricate the Ag nanoparticle line arrays in Supporting Information Figure S3 were obtained by applying several prestrain degrees of 20%, 35%, and 50% in the fabrication step of the buckling templates and the corresponding widths of Ag nanoparticle templates were 4.33, 3.58, and  $3.19 \mu\text{m}$ , respectively.

Figure 4a exhibits a top-view AFM image of Ag nanoparticles deposited on the trough of a template; the corresponding cross-sectional graph is also displayed. The obtained buckling structure can be utilized as a template for the assembly of patterned nanoparticles through dip-coating under proper conditions. The use of dip-coating in template-assisted self-assembly to prepare well-guided nanoparticle arrays has been reported by several researchers. Lu et al. investigated the strength of an anisotropic wavy structure as a self-assembly template, and nanoparticles were found to be confined in the troughs of the structures after dip-coating.<sup>36</sup> Because capillary forces were stronger in the troughs of the anisotropic buckling template due to its wavy structure as shown in Figure 4b, Ag nanoparticles were selectively assembled in the troughs of the template.

Here, a surface treatment to produce a hydrophilic surface on the target substrate was critically important for successful transfer of the Ag nanoparticles. Hanske et al. demonstrated the role and effect of surface wettability of the substrate in the transfer process of chemically treated organic nanoparticles.<sup>37</sup> During the drying step to remove water, the Ag nanoparticles were released from the surface of PS layer with the assistance of capillary forces from the water. Figure 5b shows well-defined Ag nanoparticle line arrays transferred from a buckling template to a Si substrate that was treated to induce sufficient surface tension and thus generate capillary forces with a water contact angle  $\theta < 10^\circ$ . The Ag nanoparticle line arrays had not only the uniform and periodic width, but also a high concentration of Ag nanoparticles in the periodic lines without utilizing glue materials. According to previous studies, the movement of nanoparticles that are fully immersed in water is significantly influenced by convective water flow.<sup>38</sup> Therefore, if hydrophilic surfaces are used as target substrates, it is expected that the Ag nanoparticles on the PS templates will be transferred by convective flow of the water toward the meniscus, which is caused by water evaporation at the air–water interface<sup>39</sup> as shown in Figure 5d. To investigate the influence of surface tension of the substrate on the transfer process, the target substrate was treated to yield a hydrophobic surface with a water contact angle  $\theta = 106^\circ$  by applying a monolayer of DTS before the transfer process. Figure 5c shows an SEM image of the surface of the hydrophobic target substrate coated with a monolayer of DTS after the transfer process. In contrast to the case of a hydrophilic substrate, which induces capillary forces, most of the Ag nanoparticles were not transferred when the



**Figure 4.** (a) AFM image of the Ag nanoparticles assembled in the troughs of the buckling structures: the graph at the bottom shows the cross-sectional topography of the AFM image (red line) and buckling template (dashed line). (b) Schematic illustration of the dip-coating process. Stronger capillary forces occur at the trough of the buckling structure.



**Figure 5.** (a) Schematic illustrations of the transfer process of Ag nanoparticle line arrays. (b, c) SEM images of the Ag nanoparticle line arrays transferred onto a Si wafer when the substrate has (b) a hydrophilic surface and (c) a hydrophobic surface. Insets are higher magnification images of each SEM image and the scale bars in inset are 500 nm. (d, e) Schematic, cross-sectional representations of panel a when the substrate has (d) a hydrophilic surface and (e) a hydrophobic surface. The yellow and white arrows indicate convective flow of water and water evaporation, respectively.

surface of the substrate was hydrophobic. Generally, for surfaces that have hydrophobic properties with a contact angle  $\theta > 90^\circ$ , capillary action does not occur in a closed tube.<sup>40</sup> When hydrophobic surfaces coated with a DTS monolayer are

used as substrates, small capillary forces might be generated only on the surface of PS as described in Figure 5e, because the DTS-coated Si substrates have surface tensions (water contact angle  $\theta = 106^\circ$ ) that are too low to generate capillary forces. Therefore, if hydrophobic surfaces are used as target substrates, convective flow of water occurs weakly, and the direction of convective flow heads toward the PS templates. As a result, it can be expected that the transfer efficiency of Ag nanoparticles is significantly reduced compared to hydrophilic surfaces. Therefore, the transfer process is mainly related to the surface wettability of the substrate, and Ag nanoparticle line arrays can be transferred to any flat substrate that has high surface tension. With this change of transfer efficiency, a tuning of the resulting structures can be achieved by varying surface wettability of the substrate (Supporting Information Figure S4); the details of the modulation process of surface wettability are described in previous report.<sup>30</sup> Additionally, by using large-area PS buckling templates, Ag nanoparticle line arrays formed over the macroscopic area can be obtained on the hydrophilic surface as shown in Figure S5 in Supporting Information.

As a potential application, we investigated the SERS performance of the fabricated Ag nanoparticle line arrays. Using R6G as a probing molecule, the Ag nanoparticle line arrays exhibited good SERS performance with a high Raman intensity. In Figure 6a, the graph shows the SERS spectra of R6G with various concentrations ranging from  $10^{-3}$  to  $10^{-12}$  M on the Ag nanoparticle line arrays. Several peaks for R6G in the graph are characterized by aromatic C–C stretching ( $1650$ ,  $1575$ ,  $1511$ , and  $1363$   $\text{cm}^{-1}$ ), C–O–C stretching ( $1312$   $\text{cm}^{-1}$ ), aromatic C–H bending ( $1183$   $\text{cm}^{-1}$ ), C–H out of plane bending ( $773$   $\text{cm}^{-1}$ ), and C–C–C ring in plane bending ( $612$   $\text{cm}^{-1}$ ).<sup>41</sup> Despite their lower concentrations of probing molecules, in the case of the R6G-coated samples with concentrations of  $10^{-9}$  M and  $10^{-12}$  M, they exhibited clear main Raman peaks. For instance, intensity ratios ( $I/I_0$ ) of the Raman peak at  $612$   $\text{cm}^{-1}$  ( $I$ ) and at Raman shift points without any peak ( $I_0$ ) were 12.78 and 9.27 in lower concentration of  $10^{-9}$  M and  $10^{-12}$  M. The performance of Ag nanoparticle line arrays as SERS substrates can be significantly affected by the transfer efficiency of Ag nanoparticles, which is related to the

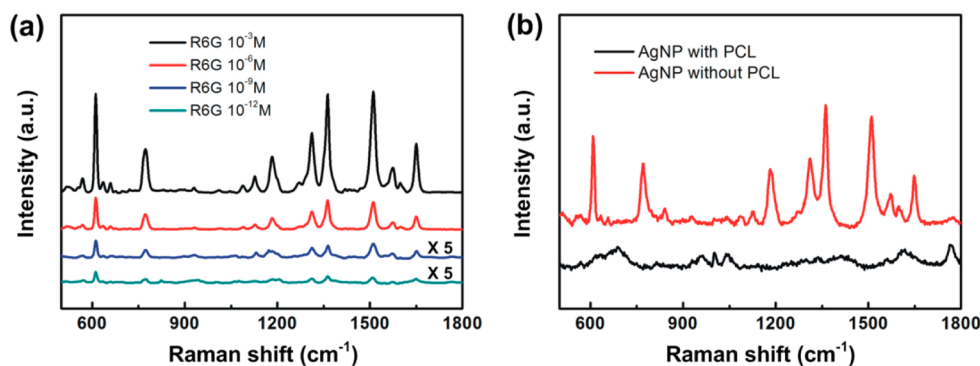


**Figure 6.** Raman spectra obtained using R6G as a probing molecule. (a) Spectra obtained using samples immersed in solutions with R6G concentrations of  $10^{-3}$ ,  $10^{-6}$ ,  $10^{-9}$ , and  $10^{-12}$  M. (b) Spectra acquired from samples with and without PCL as a glue material; R6G with a concentration of  $10^{-6}$  M was used as a probing molecule.

surface tension of the target substrates. In the case of hydrophobic surfaces, since the density of Ag nanoparticles on line arrays becomes very low compared to that of hydrophilic surfaces, the SERS performance of Ag nanoparticle line arrays on hydrophobic surfaces was significantly decreased as shown in Supporting Information Figure S6. Similarly, the main Raman peaks of NBA and BPE obtained at various concentrations (Supporting Information Figure S7) are in good agreement with those reported in the literature.<sup>42,43</sup> Despite the low laser power of  $20 \mu\text{W}$  and short exposure time of 1 s, the Ag nanoparticle line arrays displayed an excellent SERS performance for various probing molecules. Furthermore, the SERS results can be improved by increasing integration time of Raman measurements as shown in Supporting Information Figure S8. In Figure 6b, the Raman spectra show the effect of glue materials on the performance of the SERS substrate. Here, PCL was used as a glue material in the transfer process for Ag nanoparticle line arrays. In contrast to the findings obtained for Ag nanoparticle line arrays without a PCL layer, most of the main peaks of the probing molecules (R6G) with a concentration of  $10^{-6}$  M were not observed for Ag nanoparticle line arrays with a PCL layer. Because it is difficult to transfer the Ag nanoparticles located deep inside the grooves of the buckling structures in conventional adhesion-based transfer techniques, the density of Ag nanoparticles in line arrays was much lower than that of the capillary-induced transfer process adopted in our work as shown in Supporting Information Figure S9. In addition to the low density of Ag nanoparticles in line arrays, PCL layers have a detrimental effect on the SERS intensity because the Ag nanoparticles were buried in the PCL layer on the substrates during the annealing step of glue materials-based transfer process. The results demonstrate that glue-free printing of Ag nanoparticle arrays can be used in various bioanalysis and biosensor applications.

## CONCLUSIONS

In summary, well-defined Ag nanoparticle line arrays were prepared on flat substrates using anisotropic buckling templates and a transfer process that exploits capillary forces. The wavelengths of the anisotropic buckling templates employed for the assembly of Ag nanoparticles could be adjusted by changing the degree of prestrain in the fabrication step. Through dip-coating, the Ag nanoparticles were assembled in the troughs of the templates, and the resulting Ag nanoparticle line arrays assembled on the templates were successfully transferred onto a hydrophilic substrate. Because capillary forces resulting from

the addition of water are used to transfer the Ag nanoparticle line arrays in the transfer process, our method does not require additional chemical treatments or glue materials that are generally used to induce adhesion between nanoparticles and substrates. Furthermore, the wavelengths of the Ag nanoparticle line arrays assembled on the substrate could be adjusted through the use of various templates with different wavelengths. We demonstrated the excellent performance of the Ag nanoparticle line arrays as a SERS active substrate by employing various probing molecules such as R6G, NBA, and BPE. Our results are expected to be useful in many optical, electrical, and biosensor applications.

## ASSOCIATED CONTENT

### Supporting Information

FTIR spectrum of Ag nanoparticles after multiple centrifugation steps for remove of PVP. SEM images of Ag nanoparticle line arrays before and after dipping step and transferred Ag nanoparticle line arrays when various templates were used. SEM images of Ag nanoparticle line arrays on the substrates with various surface tensions and large area Ag nanoparticle line arrays. Raman spectra for other probing molecules and R6G obtained from the Ag nanoparticle line array substrates on hydrophilic and hydrophobic surfaces. Raman spectra for R6G with various concentrations. SEM image of Ag nanoparticle line arrays on a PCL layer. This material is available free of charge via the Internet at <http://pubs.acs.org>.

## AUTHOR INFORMATION

### Corresponding Author

\*Tel: +82-2-2123-5767. Fax: +82-2-313-2879. E-mail: taeyoon.lee@yonsei.ac.kr.

### Notes

The authors declare no competing financial interest.

## ACKNOWLEDGMENTS

This work was supported by the Priority Research Centers Program through the National Research Foundation of Korea (NRF) funded by the Ministry of Education, Science and Technology (2012-0006689) and by the Converging Research Center Program through the Ministry of Science, ICT, and Future Planning, Korea (2013K000183). This work was also supported by the National Research Foundation of Korea (NRF) grant funded by the Korea government (MEST) (No. 2011-0028594)

## REFERENCES

- (1) John, S. Strong Localization of Photons in Certain Disordered Dielectric Superlattices. *Phys. Rev. Lett.* **1987**, *58*, 2486–2489.
- (2) Shipway, A. N.; Katz, E.; Willner, I. Nanoparticle Arrays on Surfaces for Electronic, Optical, and Sensor Applications. *ChemPhysChem* **2000**, *1*, 18–52.
- (3) Alvarez-Puebla, R. A.; Agarwal, A.; Manna, P.; Khanal, B. P.; Aldeanueva-Potel, P.; Carbó-Argibay, E.; Pazos-Pérez, N.; Vigderman, L.; Zubarev, E. R.; Kotov, N. A.; Liz-Marzán, L. M. Gold Nanorods 3D-supercrystals as Surface Enhanced Raman Scattering Spectroscopy Substrates for the Rapid Detection of Scrambled Prions. *Proc. Natl. Acad. Sci. U.S.A.* **2011**, *108*, 8157–8161.
- (4) Reineck, P.; Lee, G. P.; Brick, D.; Karg, M.; Mulvaney, P.; Bach, U. A Solid-State Plasmonic Solar Cell via Metal Nanoparticle Self-Assembly. *Adv. Mater.* **2012**, *24*, 4750–4755.
- (5) Haynes, C. L.; Van Duyne, R. P. Nanosphere Lithography: A Versatile Nanofabrication Tool for Studies of Size-Dependent Nanoparticle Optics. *J. Phys. Chem. B* **2001**, *105*, 5599–5611.
- (6) Yi, D. K.; Kim, M. J.; Turner, L.; Breuer, K. S.; Kim, D.-Y. Colloid Lithography-Induced Polydimethylsiloxane Microstructures and their Application to Cell Patterning. *Biotechnol. Lett.* **2006**, *28*, 169–173.
- (7) Fuhrmann, B.; Leipner, H. S.; Höche, H.-R.; Schubert, L.; Werner, P.; Gösele, U. Ordered Arrays of Silicon Nanowires Produced by Nanosphere Lithography and Molecular Beam Epitaxy. *Nano Lett.* **2005**, *5*, 2524–2527.
- (8) Ko, H.; Singamaneni, S.; Tsukruk, V. V. Nanostructured Surfaces and Assemblies as SERS Media. *Small* **2008**, *4*, 1576–1599.
- (9) Stein, A.; Schroden, R. C. Colloidal Crystal Templating of Three-Dimensionally Ordered Macroporous Solids: Materials for Photonics and Beyond. *Curr. Opin. Solid State Mater. Sci.* **2001**, *5*, 553–564.
- (10) Fan, J. A.; Wu, C.; Bao, K.; Bao, J.; Bardhan, R.; Halas, N. J.; Manoharan, V. N.; Nordlander, P.; Shvets, G.; Capasso, F. Self-Assembled Plasmonic Nanoparticle Clusters. *Science* **2010**, *328*, 1135–1138.
- (11) Zhu, J.; Li, M.; Rogers, R.; Meyer, W.; Ottewill, R. H.; Russel, W. B.; Chaikin, P. M. Crystallization of Hard-Sphere Colloids in Microgravity. *Nature* **1997**, *387*, 883–885.
- (12) Gu, Z.-Z.; Fujishima, A.; Sato, O. Fabrication of High-Quality Opal Films with Controllable Thickness. *Chem. Mater.* **2002**, *14*, 760–765.
- (13) Chiou, P. Y.; Ohta, A. T.; Wu, M. C. Massively Parallel Manipulation of Single Cells and Microparticles using Optical Images. *Nature* **2005**, *436*, 370–372.
- (14) Jiang, L.; Sun, Y.; Nowak, C.; Kibrom, A.; Zou, C.; Ma, J.; Fuchs, H.; Li, S.; Chi, L.; Chen, X. Patterning of Plasmonic Nanoparticles into Multiplexed One-Dimensional Arrays Based on Spatially Modulated Electrostatic Potential. *ACS Nano* **2011**, *5*, 8288–8294.
- (15) Yang, B.; Lu, N.; Huang, C.; Qi, D.; Shi, G.; Xu, H.; Chen, X.; Dong, B.; Song, W.; Zhao, B.; Chi, L. Electrochemical Deposition of Silver Nanoparticle Arrays with Tunable Density. *Langmuir* **2009**, *25*, 55–58.
- (16) Lohmüller, T.; Aydin, D.; Schwieder, M.; Morhard, C.; Louban, I.; Pacholski, C.; Spatz, J. P. Nanopatterning by Block Copolymer Micelle Nanolithography and Bioinspired Applications. *Biointerphases* **2011**, *6*, MR1–MR12.
- (17) Xia, Y.; Yin, Y.; Lu, Y.; McLellan, J. Template-Assisted Self-Assembly of Spherical Colloids into Complex and Controllable Structures. *Adv. Funct. Mater.* **2003**, *13*, 907–918.
- (18) Yin, Y.; Lu, Y.; Gates, B.; Xia, Y. Template-Assisted Self-Assembly: A Practical Route to Complex Aggregates of Monodispersed Colloids with Well-Defined Sizes, Shapes, and Structures. *J. Am. Chem. Soc.* **2001**, *123*, 8718–8729.
- (19) Ozin, G. A.; Yang, S. M. The Race for the Photonic Chip: Colloidal Crystal Assembly in Silicon Wafers. *Adv. Funct. Mater.* **2001**, *11*, 95–104.
- (20) Seo, J.; Lee, H.; Lee, S.; Lee, T. I.; Myoung, J.-M.; Lee, T. Direct Gravure Printing of Silicon Nanowires Using Entropic Attraction Forces. *Small* **2012**, *8*, 1614–1621.
- (21) Velev, O. D.; Gupta, S. Materials Fabricated by Micro- and Nanoparticle Assembly—The Challenging Path from Science to Engineering. *Adv. Mater.* **2009**, *21*, 1897–1905.
- (22) Ramanathan, M.; Kilbey, S. M., II; Ji, Q.; Hill, J. P.; Ariga, K. Materials Self-Assembly and Fabrication in Confined Spaces. *J. Mater. Chem.* **2012**, *22*, 10389–10405.
- (23) Fang, J. Ordered Arrays of Self-Assembled Lipid Tubules: Fabrication and Applications. *J. Mater. Chem.* **2007**, *17*, 3479–3484.
- (24) Mendes, P. M.; Jacke, S.; Critchley, K.; Plaza, J.; Chen, Y.; Nikitin, K.; Palmer, R. E.; Preece, J. A.; Evans, S. D.; Fitzmaurice, D. Gold Nanoparticle Patterning of Silicon Wafers Using Chemical e-Beam Lithography. *Langmuir* **2004**, *20*, 3766–3768.
- (25) Ling, X. Y.; Phang, I. Y.; Maijenburg, W.; Schönherr, H.; Reinhoudt, D. N.; Vancso, G. J.; Huskens, J. Free-Standing 3D Supramolecular Hybrid Particle Structures. *Angew. Chem., Int. Ed.* **2009**, *48*, 983–987.
- (26) Hyun, D. C.; Moon, G. D.; Cho, E. C.; Jeong, U. Repeated Transfer of Colloidal Patterns by Using Reversible Buckling Process. *Adv. Funct. Mater.* **2009**, *19*, 2155–2162.
- (27) Wang, Y.; Yan, B.; Chen, L. SERS Tags: Novel Optical Nanoprobes for Bioanalysis. *Chem. Rev.* **2012**, *113*, 1391–1428.
- (28) Schweikart, A.; Pazos-Pérez, N.; Alvarez-Puebla, R. A.; Fery, A. Controlling Inter-nanoparticle Coupling by Wrinkle-Assisted Assembly. *Soft Matter* **2011**, *7*, 4093–4100.
- (29) Cialla, D.; März, A.; Böhme, R.; Theil, F.; Weber, K.; Schmitt, M.; Popp, J. Surface-Enhanced Raman Spectroscopy (SERS): Progress and Trends. *Anal. Bioanal. Chem.* **2012**, *403*, 27–54.
- (30) Seo, J.; Lee, S.; Lee, J.; Lee, T. Guided Transport of Water Droplets on Superhydrophobic–Hydrophilic Patterned Si Nanowires. *ACS Appl. Mater. Interfaces* **2011**, *3*, 4722–4729.
- (31) Seo, J.; Lee, S.; Han, H.; Jung, H. B.; Hong, J.; Song, G.; Cho, S. M.; Park, C.; Lee, W.; Lee, T. Gas-Driven Ultrafast Reversible Switching of Super-Hydrophobic Adhesion on Palladium-Coated Silicon Nanowires. *Adv. Mater.* **2013**, *25*, 4139–4144.
- (32) Korte, K. E.; Skrabalak, S. E.; Xia, Y. Rapid Synthesis of Silver Nanowires through a CuCl- or CuCl<sub>2</sub>-Mediated Polyol Process. *J. Mater. Chem.* **2008**, *18*, 437–441.
- (33) Kirkland, A. I.; Jefferson, D. A.; Duff, D. G.; Edwards, P. P.; Gameson, I.; Johnson, B. F. G.; Smith, D. J. Structural Studies of Trigonal Lamellar Particles of Gold and Silver. *Proc. R. Soc. London A, Math Phys. Sci.* **1993**, *440*, 589–609.
- (34) Puntès, V. F.; Krishnan, K. M.; Alivisatos, A. P. Colloidal Nanocrystal Shape and Size Control: The Case of Cobalt. *Science* **2001**, *291*, 2115–2117.
- (35) Jiang, H.; Khang, D.-Y.; Song, J.; Sun, Y.; Huang, Y.; Rogers, J. A. Finite Deformation Mechanics in Buckled Thin Films on Compliant Supports. *Proc. Natl. Acad. Sci. U.S.A.* **2007**, *104*, 15607–15612.
- (36) Lu, C.; Möhwald, H.; Fery, A. A Lithography-free Method for Directed Colloidal Crystal Assembly Based on Wrinkling. *Soft Matter* **2007**, *3*, 1530–1536.
- (37) Hanske, C.; Müller, M. B.; Bieber, V.; Tebbe, M.; Jessl, S.; Wittmann, A.; Fery, A. The Role of Substrate Wettability in Nanoparticle Transfer from Wrinkled Elastomers: Fundamentals and Application toward Hierarchical Patterning. *Langmuir* **2012**, *28*, 16745–16750.
- (38) Denkov, N. D.; Velev, O. D.; Kralchevsky, P. A.; Ivanov, I. B.; Yoshimura, H.; Nagayama, K. Mechanism of Formation of Two-Dimensional Crystals from Latex Particles on Substrates. *Langmuir* **1992**, *8*, 3183–3190.
- (39) Kraus, T.; Malaquin, L.; Schmid, H.; Riess, W.; Spencer, N. D.; Wolf, H. Nanoparticle Printing with Single-Particle Resolution. *Nat. Nanotechnol.* **2007**, *2*, 570–576.
- (40) Dreyer, M.; Delgado, A.; Path, H.-J. Capillary Rise of Liquid between Parallel Plates under Microgravity. *J. Colloid Interface Sci.* **1994**, *163*, 158–168.
- (41) Li, H. B.; Liu, P.; Liang, Y.; Xiao, J.; Yang, G. W. Super-SERS-Active and Highly Effective Antimicrobial Ag Nanodendrites. *Nano-scale* **2012**, *4*, 5082–5091.

(42) Álvarez-Puebla, R. A.; Contreras-Cáceres, R.; Pastoriza-Santos, I.; Pérez-Juste, J.; Liz-Marzán, L. M. Au@pNIPAM Colloids as Molecular Traps for Surface-Enhanced, Spectroscopic, Ultra-Sensitive Analysis. *Angew. Chem., Int. Ed.* **2009**, *48*, 138–143.

(43) Singh, J. P.; Lanier, T. E.; Zhu, H.; Dennis, W. M.; Tripp, R. A.; Zhao, Y. Highly Sensitive and Transparent Surface Enhanced Raman Scattering Substrates Made by Active Coldly Condensed Ag Nanorod Arrays. *J. Phys. Chem. C* **2012**, *116*, 20550–20557.